Enhancing hydrogen spillover and oxygen vacancies in $CdZrO_x$ solid solution catalysts via the synergistic effect of Cu and Ga for efficient CO_2 hydrogenation to methanol

Yu Zhou[1], Ke Zhuang[2], Yun Xu[2], Kai Shen[1], Yaping Zhang[1]*, Tingyu Zhu[3], Wenqing Xu[3]*

[1]*Key Laboratory of Energy Thermal Conversion and Control of Ministry of Education, School of Energy and Environment, Southeast University, Nanjing 210096, Jiangsu, China*

[2]*State Power Environmental Protection Research Institute, Nanjing 210031, Jiangsu, China*

[3]*Institute of Process Engineering, Chinese Academy of Sciences, Beijing 100190, China*

* Corresponding author. **Yaping Zhang**, E-mail address: amflora@seu.edu.cn, **Wenqing Xu**, E-mail address: wqxu@ipe.ac.cn

Catalyst characterization

Catalyst chemical compositions were measured on a Thermo Fisher iCAP PRO inductively coupled plasma optical emission spectrometry (ICP-OES). The X-ray diffraction (XRD) patterns of all the samples were determined by a Bruker D8 Advance X-ray diffractometer over the 2θ range of 5-90° with the scanning speed was set as 5 °/min. The diffractometer was operated at 40 kV and 40 mA with CuKα irradiation (λ = 0.15406 nm). The Raman spectra were collected on a Horiba LabRAM HR Evolution Micro-Raman Spectrometer with a 532 nm light source. High resolution transmission electron microscope (HRTEM) with an energy dispersive spectrometer (EDS) was performed using Thermo Fisher Talos P200X G2 microscope operated at an accelerating voltage of 200 kV. X-ray photoelectron spectroscopy (XPS) with a Thermo Scientific K-Alpha+ spectrometer equipped with an Al Ka X-ray source (hν = 1486.6 eV) were used to measure the surface atomic states of catalysts. The binding energy of Cu 2p, Ga 2p, Cd 3d, Zr 3d and O 1s was calibrated according to the surface contamination C 1s (284.8 eV). Nitrogen physisorption was carried out using a Micromeritics ASAP 2460 system to analyze the specific surface area and pore structure according to the standard Brunauer-Emmett-Teller (BET) method and the Barrett-Joyner-Helenda (BJH) desorption branch. The samples were first degassed in vacuum at 300 °C for 180 min before the measurement. Electron Paramagnetic Resonance (EPR) tests were carried out using a Bruker EMXplus X-band EPR spectrometer (Bruker BioSpin, Rheinstetten, Germany), which was used to analyse species with a paramagnetic response. Spectra were acquired at a temperature of -196 °C with a signal scan range of 2600 Gauss-4200 Gauss.

The H_2 temperature-programmed reduction (H_2-TPR) profiles were collected on a chemisorption analyzer (BSD-Chem C200) equipped with a TCD detector. Firstly, 50 mg of the catalyst was pretreated at 300 °C for 60 min under an Ar flow (30 mL/min). After cooling to 30 °C, the gas was switched to 10% H_2/Ar stream (30 mL/min) to conduct the temperature-programmed reduction from 30 °C to 800 °C with a heating rate of 10 °C/min. The H_2 consumption was detected by TCD in real time. For the CO_2/H_2/O_2-TPD analysis, Specifically, 50 mg of the catalyst was reduced in-situ at 300

°C for 60 min under a stream of Ar or He (30 mL/min), and then cooled to room temperature. It was then switched to a 10% H_2/Ar, 10% CO_2/He, or 10% O_2/He stream at 30 mL/min for 60 min, flushed by Ar or He stream (30 mL/min) at 30 °C for 30 min to remove physically adsorbed molecules. Afterward, the sample was flushed by the Ar or He stream at 30 mL/min for 40 min until a stable baseline was gained. Lastly, the TPD test is performed from 30 °C to 800 °C at a ramp rate of 10 °C/min. The signal of CO_2/H_2/O_2 desorption was detected using a TCD detector.

The N_2O titration experiment was conducted on a chemisorption analyzer (BSD-Chem C200) equipped with a thermal conductivity detector (TCD). Firstly, 50 mg of the sample was placed in a U-shaped quartz tube, and subjected to a drying pretreatment by program heating from room temperature to 200 °C at a rate of 10 °C/min, with Ar gas flow (30 mL/min) purging for 60 min. After cooling to room temperature, a 10% H_2/Ar gas mixture (30 mL/min) was introduced for 60 min until the baseline stabilized. Then, the sample was heated from room temperature to 300 °C at a rate of 10 °C/min in a 10% H_2/Ar gas flow. The reducing gas was detected by TCD, and the peak area X was calculated by recording the curve. Without removing the sample, it was cooled to room temperature and purged with high-purity Ar for 30 min. After heating to 50 °C, a 10% N_2O/He gas mixture was introduced to oxidize the surface Cu until the detector signal no longer fluctuated (45 min). Ar continued to purge for 30 min to remove physically adsorbed N_2O. Then, the gas was switched to 10% H_2/Ar mixture, and purging was continued for 60 min until the baseline became stable. The sample was heated from room temperature to 300 °C at a rate of 10 °C/min in a 10% H_2/Ar gas flow. The reducing gas was detected by TCD, and the peak area Y was calculated by recording the curve.

$$D_{Cu}(\%) = \frac{2Y}{X}$$

$$S_{Cu} = \frac{2 \times Y \times N_a}{X \times M_{Cu} \times A}$$

$$d_{Cu}(nm) = \frac{6 \times 10^3}{S_{Cu}\rho_{Cu}}$$

Where Na is Avogadro's constant (6.02×10^{23} atom per mol); M_{Cu} is the Cu molar mass (63.55 g mol^{-1}); A is the number of Cu surface atoms per unit area (1.46×10^{19} atom Cu/m^2); ρ_{Cu} is the density of Cu, which is 8.92 g/cm^3.

For the H_2-D_2 isotopic exchange reaction, 50 mg of the catalyst was pretreated with a 10 vol % H_2/Ar gas flow (30 mL/min) at 300 °C for 2 h. Subsequently, the system was purged with an Ar gas flow (30 mL/min) at the same temperature for 30 min to remove unreacted gases and water. The system was then cooled to room temperature under an Ar atmosphere. After that, a gas mixture of 10 vol % H_2/10 vol % D_2/Ar (30 mL/min) was injected into the reactor. Once the system stabilized at room temperature, the sample was heated from room temperature to 600 °C at a rate of 10 °C/min. The signals of H_2 (m/z=2), D_2 (m/z=4), and HD (m/z=3) were recorded using a mass spectrometer (Microtrac BELCat II, Japan).

In situ DRIFTS were conducted at the Nicolet 6700 spectrometer (Thermo Fisher Scientific, USA) equipped with a liquid-nitrogen-cooled MCT detector and a high temperature reaction cell. The spectra in the range of 1000-4000 cm^{-1} were collected at a resolution of 4cm^{-1} by accumulating 64 scans. Typically, catalysts were placed into the chamber and pretreated with a stream of H_2 at 300 °C for 60 min, and then cooled to the target temperature under a nitrogen atmosphere. The background spectra were measured under N_2 flow at the target temperature. At the target temperature, the catalysts were first in a pure CO_2 atmosphere, then a mixture of reaction gases (H_2:CO_2 = 3:1), and finally H_2. In order to obtain time-dependent spectra in different atmospheres, the IR signals were taken at regular intervals in different gas environments until the adsorption was saturated. Moreover, the spectra were recorded as a function of temperature under the same pretreatment conditions and in a reactive gas atmosphere

of CO_2 + H_2 (H_2:CO_2 = 3:1). In-situ H_2 FTIR spectroscopy was used to identify Ga-H species. The fresh catalyst was treated with Ar at 300 °C for 30 min to remove absorbed moisture and impurities, followed by cooling to room temperature under an Ar atmosphere. After collecting the background spectrum, the sample was exposed to a flow of H_2 during the scanning process. The temperature was then raised to 250 °C at a heating rate of 10 °C/min, with spectra collected simultaneously. In addition, CO-IR measurements were performed on the device. Typically, the samples were reduced in situ with pure H_2 at 300 °C for 40 min (30 mL/min) and then cooled to 30 °C in a He atmosphere. Next, background spectra were collected under a stream of He gas (30 mL/min). Subsequently, the gas was switched to 5% CO/He and continued for 30 min to saturate the catalyst. Finally, the gas mixture was replaced with pure He and purged for another 30 min to remove adsorbents from the sample surface. Finally, the sample spectral signal was collected.

Table S1. Catalytic hydrogenation performance of the various catalyst. Reaction conditions: 3 MPa, H_2/CO_2 = 3:1, GHSV = 24000 mL/g_{cat}·h, 320 °C.

Catalyst	X_{CO2} (%)	Production Selectivity (%)			CH_3OH Yield
		CH_3OH	CH_4	CO	(mg/(g_{cat}·h))
$CdZrO_x$	3.7	69.9	0.2	29.8	230
$5GaCdZrO_x$	4.7	69.3	0.2	30.4	283
$2CuCdZrO_x$	2.8	71.7	0.3	27.9	179
$0.2CuGaCdZrO_x$	4.5	77.0	0.2	22.7	312
$2CuGaCdZrO_x$	6.1	68.4	0.2	31.3	373
$5CuGaCdZrO_x$	5.3	67.5	0.2	32.2	312
$10CuGaCdZrO_x$	2.5	63.3	0.4	36.2	143

Table S2. Comparison of catalytic performance over $2CuGaCdZrO_x$ solid solution catalyst with other reported solid solution catalysts and Cu-based catalysts in the literature for CO_2 hydrogenation to methanol.

Catalyst	Test condition	CO_2 Conv. (%)	CH_3OH Sel. (%)	STY_{CH3OH} (mg/g_{cat}·h)	Ref.
42.0%In-	5 MPa, 300℃, H_2/CO_2=3:1,	11.0	80.1	370.0	[1]

$ZnZrO_x$	GHSV=12000 mL/g·h				
$ZnZrO_x$	5 MPa, 325℃, H_2/CO_2=3:1, GHSV=24000 mL/g·h	5.2	72.2	273.4	[2]
5.0%Zn-$CdZrO_x$	5 MPa, 320℃, H_2/CO_2=4:1, GHSV=24000 mL/g·h	8.5	80.8	375.0	[3]
$2CuGaZrO_x$	3 MPa, 300℃, H_2/CO_2=3:1, GHSV=6000 mL/g·h	8.3	87.0	~155.0	[4]
ZnO-ZrO_2 (Zn/Zr=1)	3.0 MPa, 320℃, H_2/CO_2=3:1, GHSV=18000 mL/g·h	5.7	70.0	246.4	[5]
$GaZrO_x$	2.0 MPa, 300℃, H_2/CO_2=3:1, GHSV=24000 h^{-1}	2.4	75.0	140.0	[6]
15ZnZr-600	2.0 MPa, 300℃, H_2/CO_2=3:1, GHSV=9000 mL/g·h	5.5	75.1	105.6	[7]
In_2O_3/m-ZrO_2	5.0 MPa, 280℃, H_2/CO_2=4:1, GHSV=24000 mL/g·h	4.7	84.0	268.8	[8]
0.2CuZnZr	4.5 MPa, 290℃, H_2/CO_2=3:1, GHSV=10800 mL/g·h	6.0	78.4	167.0	[9]
$CuCeZrO_x$	3.0 MPa, 240℃, H_2/CO_2=3:1, GHSV=30000 mL/g·h	4.1	55.3	192.0	[10]
$ZnZrO_x$-MD	3.0 MPa, 320℃, H_2/CO_2=3:1, GHSV=24000 mL/g·h	5.4	77.2	~341.0	[11]
$ZnZrO_x$-TD		3.8	80.0	~245.0	
CCZ-CP	3.0 MPa, 300℃, H_2/CO_2=3:1, GHSV=12000 h^{-1}	16.3	17.5	129.0	[12]
CCZ-HM		7.9	66.3	224.0	
$Cu/Ce_{0.2}Zr_{0.8}O_2$	3.0 MPa, 280℃, H_2/CO_2=3:1, GHSV=12000 h^{-1}	5.7	94.4	231.4	[13]
10In300Zr400	5.0 MPa, 310℃, H_2/CO_2=3:1, GHSV=12000 mL/g·h	10.4	73.1	302.0	[14]
ZrO_2(30)-In_2O_3	5.0 MPa, 180℃, H_2/CO_2=4:1, GHSV=N.A.	N.A.	90.0	44.8	[15]
CuZn	3.0 MPa, 230℃, H_2/CO_2=3:1, GHSV=6000 mL/g·h	15.8	35.1	173.0	[16]
$Cu/1GaZrO_x$	3.0 MPa, 300℃, H_2/CO_2=3:1, GHSV=18000 mL/g·h	6.2	83.4	334.0	[17]
CuZr-1	3.0 MPa, 260℃, H_2/CO_2=3:1, GHSV=15000 mL/g·h	9.0	72.1	361.6	[18]
CZZ(5:4:1)	3.0 MPa, 240℃, H_2/CO_2=3:1, GHSV=4500 mL/g·h	17.0	~42.0	112.9	[19]
10Cu/ZnCr-3.5	2 MPa, 250℃, H_2/CO_2=3:1, GHSV=6000 mL/g·h	10.9	48.0	102.4	[20]
$2CuGaCdZrO_x$	3 MPa, 320℃, H_2/CO_2=3:1, GHSV=24000 mL/g·h	6.1	68.4	373.0	This work

Table S3. Activation energies of various catalysts.

Catalyst	$Ea_{,MeOH}$ (kJ/mol)	$Ea_{,CO}$ (kJ/mol)
$CdZrO_x$	73.62	122.95
$2CuGaCdZrO_x$	37.57	132.16

$5CuGaCdZrO_x$	39.25	140.70

Table S4. ICP-OES analysis of the catalysts.

Catalyst	Cu (atom%)	Catalyst	Cu (atom%)
$0.2CuGaCdZrO_x$	0.22	$5CuGaCdZrO_x$	4.69
$2CuGaCdZrO_x$	2.07	$10CuGaCdZrO_x$	9.37
$2CuCdZrO_x$	1.87		

Table S5. Textural properties of as-prepared catalysts.

Catalyst	S_{BET} (m^2/g)	Pore Volume (cm^3/g)	Pore Size (nm)	$D_{crystallite}$[a] (nm)	D_{Cu}[b] (%)	d_{Cu} (nm)
$CdZrO_x$	26.9	0.0218	3.4	32.8	/	/
$5GaCdZrO_x$	52.2	0.0398	3.2	28.0	/	/
$2CuCdZrO_x$	18.0	0.0196	4.3	31.7	58.3	1.778
$0.2CuGaCdZrO_x$	25.9	0.0243	4.1	28.5	/	/
$2CuGaCdZrO_x$	42.3	0.0397	3.7	23.5	73.6	1.409
$5CuGaCdZrO_x$	34.8	0.0344	3.8	24.2	34.5	3.005
$10CuGaCdZrO_x$	20.6	0.0258	5.2	41.3	23.1	4.488

[a] Determined from XRD using the Scherrer equation.

[b] Cu dispersion was determined by N_2O chemisorption.

Table S6. Deconvolution results of O 1s XPS peaks for the reduced catalysts.

Catalyst	O species relative content (%)		
	$O_I/O_I + O_{II} + O_{III}$	$O_{II}/O_I + O_{II} + O_{III}$	$O_{III}/O_I + O_{II} + O_{III}$
$CdZrO_x$	50.7	23.8	25.5
$0.2CuGaCdZrO_x$	64.2	24.3	11.5
$2CuGaCdZrO_x$	63.1	31.1	5.8
$5CuGaCdZrO_x$	63.0	26.8	10.2

$10CuGaCdZrO_x$	60.5	20.7	18.8

Table S7. Quantitative result of the CO_2-TPD.

Catalyst	**CO_2 uptake (mmol/g)**	
$CdZrO_x$	**117 ℃** 0.0626	**392 ℃** 0.0563
$0.2CuGaCdZrO_x$	**105 ℃** 0.0740	**420 ℃** 0.1214
$2CuGaCdZrO_x$	**111 ℃** 0.1897	**419 ℃** 0.1869
$5CuGaCdZrO_x$	**114 ℃** 0.1490	**413 ℃** 0.1042
$10CuGaCdZrO_x$	**122 ℃** 0.0478	**392 ℃** 0.0260

Table S8. Quantitative result of the H_2-TPD and normalized content.

Catalyst	**Peak α-H_2 uptake (mmol/g)**	**Peak β-H_2 uptake (mmol/g)**	**Normalized content (%)**
$CdZrO_x$	/	0.0321	18.6
$5GaCdZrO_x$	/	0.0749	43.4
$2CuCdZrO_x$	0.0083	0.0333	24.1
$0.2CuGaCdZrO_x$	0.0113	0.0566	39.3
$2CuGaCdZrO_x$	0.0298	0.1429	100
$5CuGaCdZrO_x$	0.0177	0.1382	90.3
$10CuGaCdZrO_x$	0.0064	0.1084	66.5

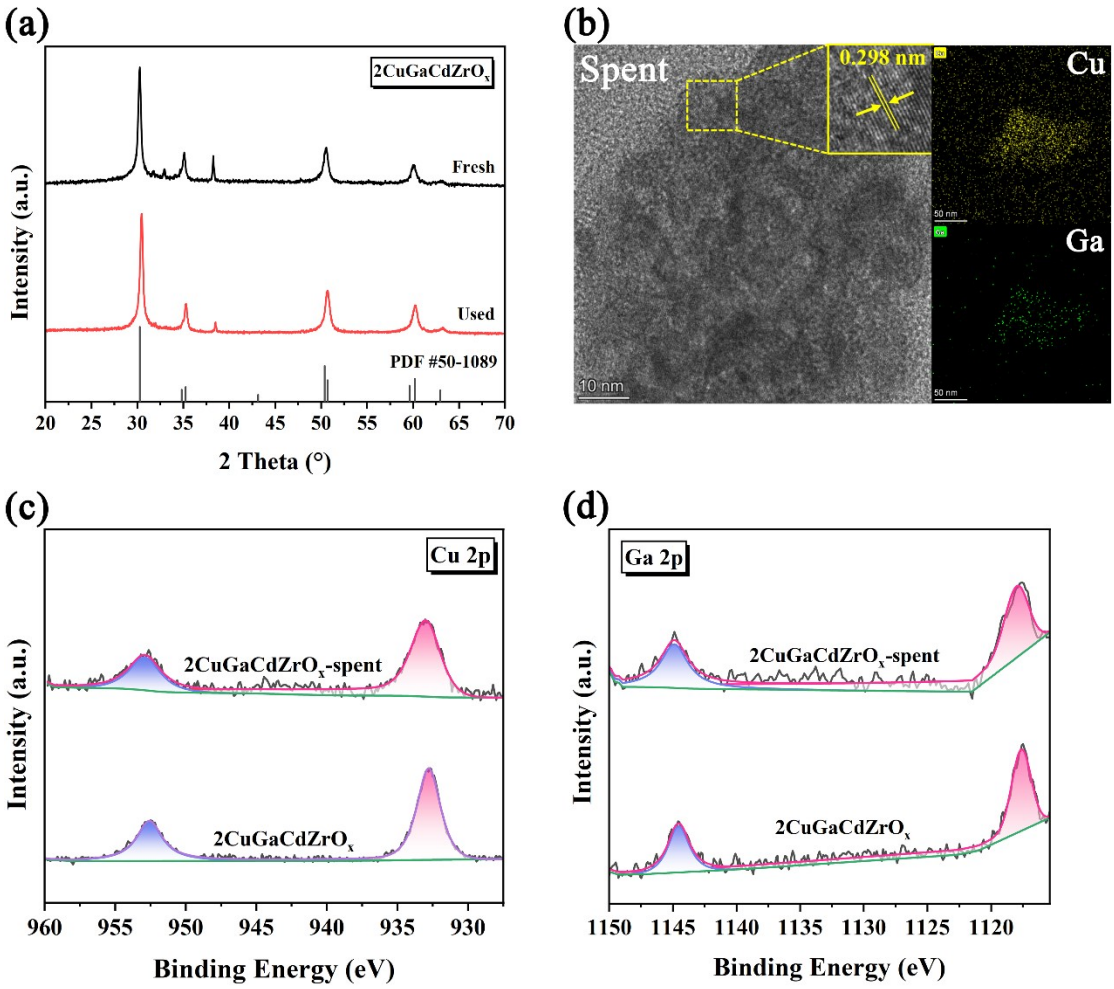

Fig. S1. The comparison of (a) XRD pattern, (b) HRTEM image with element mappings, (c) XPS spectra of Cu 2p and (d) Ga 2p between 2CuGaCdZrO$_x$ and spent 2CuGaCdZrO$_x$.

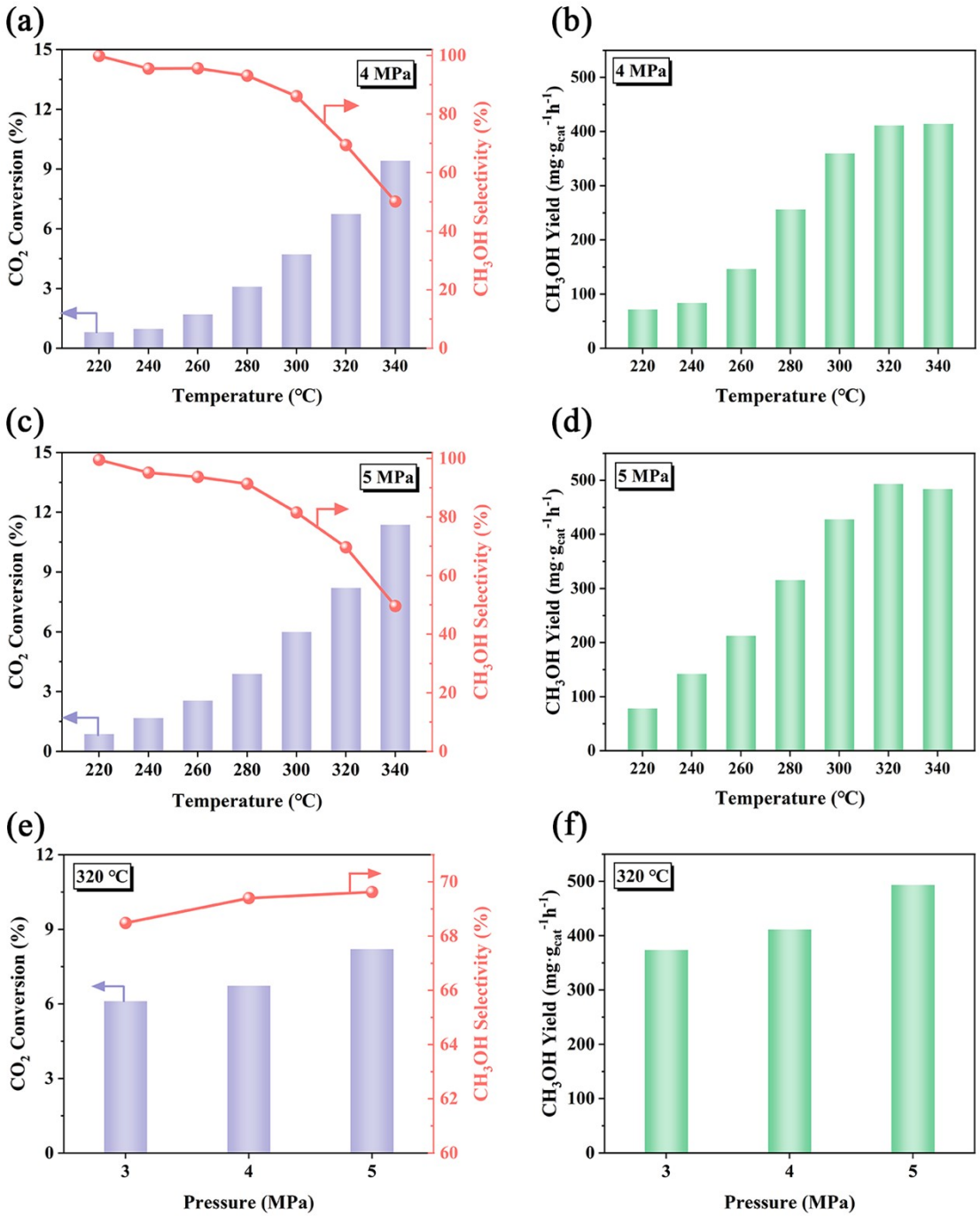

Fig. S2. (a) CO_2 conversion, methanol selectivity, and (b) methanol yield as a function of temperature over the $2CuGaCdZrO_x$ catalyst. Reaction conditions: 4 MPa, H_2/CO_2 = 3:1, GHSV = 24000 mL/g·h. (c) CO_2 conversion, methanol selectivity, and (d) methanol yield as a function of temperature over the $2CuGaCdZrO_x$ catalyst. Reaction conditions: 5 MPa, H_2/CO_2 = 3:1, GHSV = 24000 mL/g·h. (e) CO_2 conversion, methanol selectivity, and (f) methanol yield as a function of pressure over the $2CuGaCdZrO_x$ catalyst. Reaction conditions: 320 °C, H_2/CO_2 = 3:1, GHSV = 24000 mL/g·h.

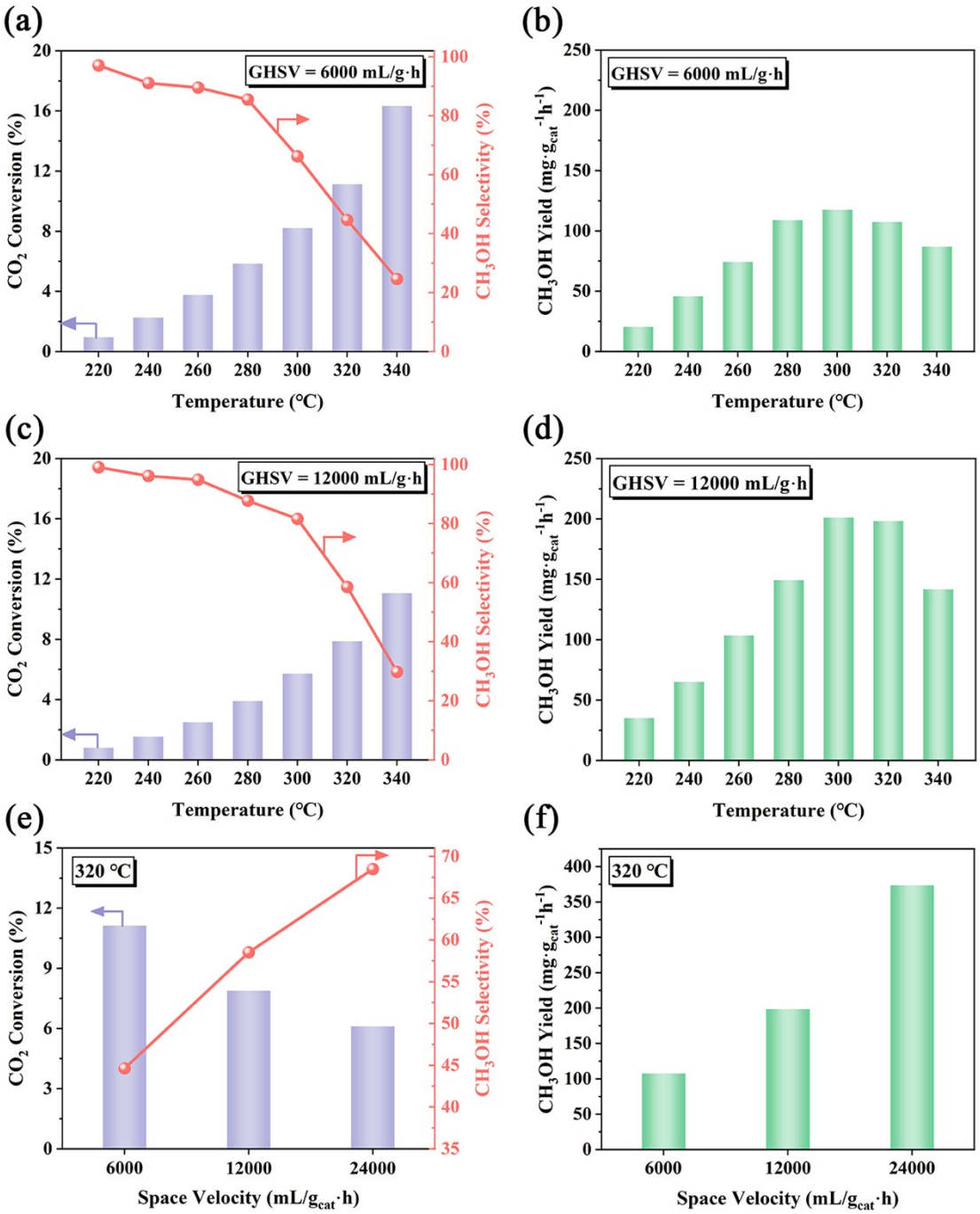

Fig. S3. (a) CO_2 conversion, methanol selectivity, and (b) methanol yield as a function of temperature over the 2CuGaCdZrO_x catalyst. Reaction conditions: 3 MPa, H_2/CO_2 = 3:1, GHSV = 6000 mL/g·h. (c) CO_2 conversion, methanol selectivity, and (d) methanol yield as a function of temperature over the 2CuGaCdZrO_x catalyst. Reaction conditions: 3 MPa, H_2/CO_2 = 3:1, GHSV = 12000 mL/g·h. (e) CO_2 conversion, methanol selectivity, and (f) methanol yield as a function of space velocity over the 2CuGaCdZrO_x catalyst. Reaction conditions: 320 °C, H_2/CO_2 = 3:1, 3 MPa.

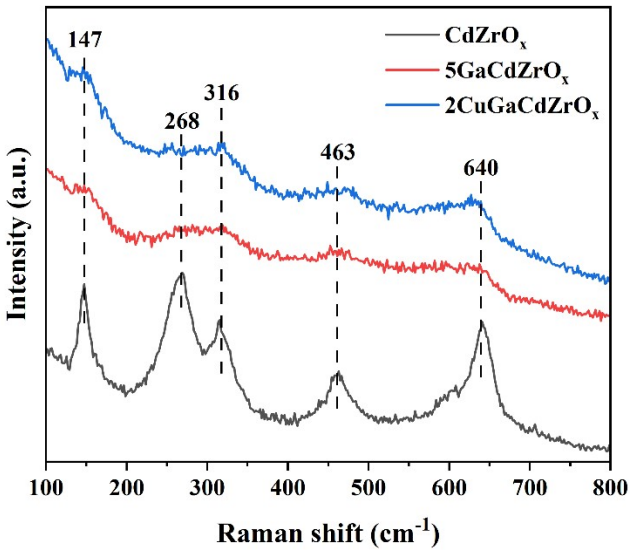

Fig. S4. Raman spectra of $CdZrO_x$, $5GaCdZrO_x$, and $2CuGaCdZrO_x$ catalysts.

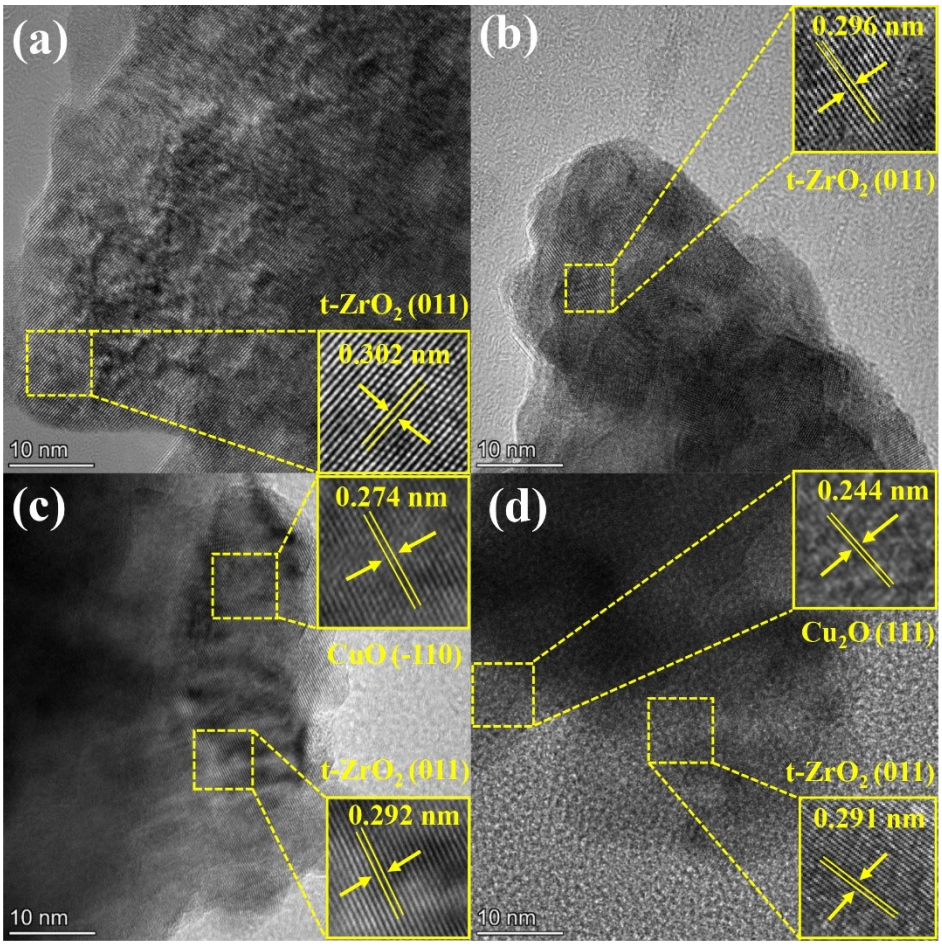

Fig. S5. The HRTEM images of (a) $0.2CuGaCdZrO_x$, (b) $2CuGaCdZrO_x$, (c) $5CuGaCdZrO_x$, and (d) $10CuGaCdZrO_x$ catalysts.

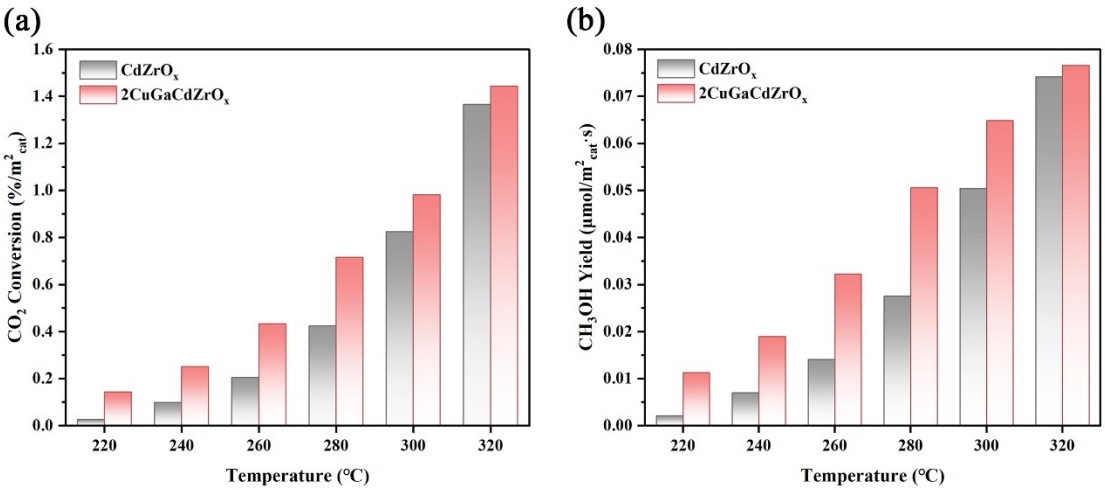

Fig. S6. The catalytic performance normalized by BET specific surface area over the reduced catalysts. (a) CO_2 conversion and (b) CH_3OH Yield. Reaction conditions: 3 MPa, H_2/CO_2 = 3:1, GHSV = 24000 mL/g_{cat}·h.

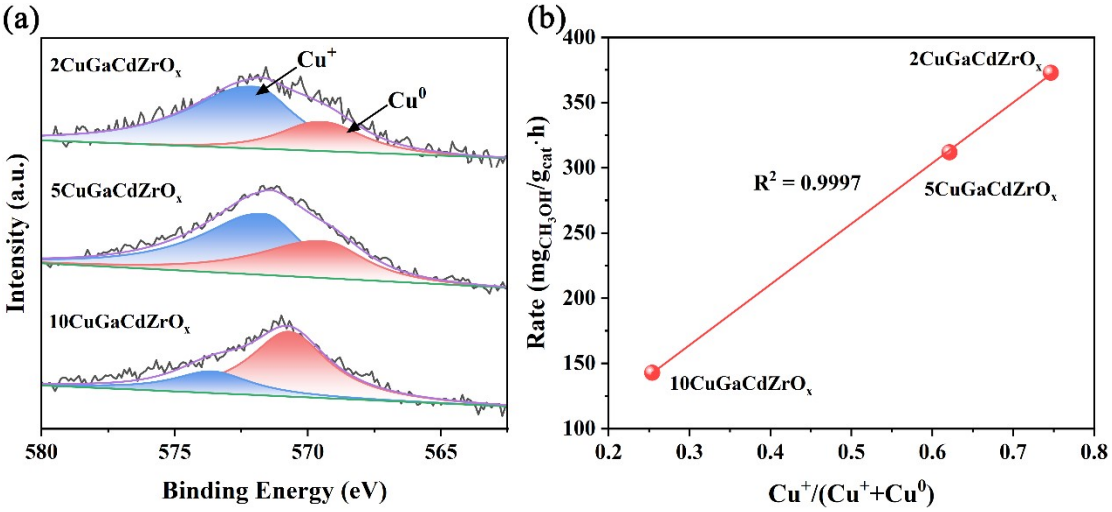

Fig. S7. (a) Cu-LMM Auger spectra and (b) $Cu^+/(Cu^+ + Cu^0)$ as a function of methanol yield of reduced 2CuGaCdZrO_x, 5CuGaCdZrO_x and 10CuGaCdZrO_x.

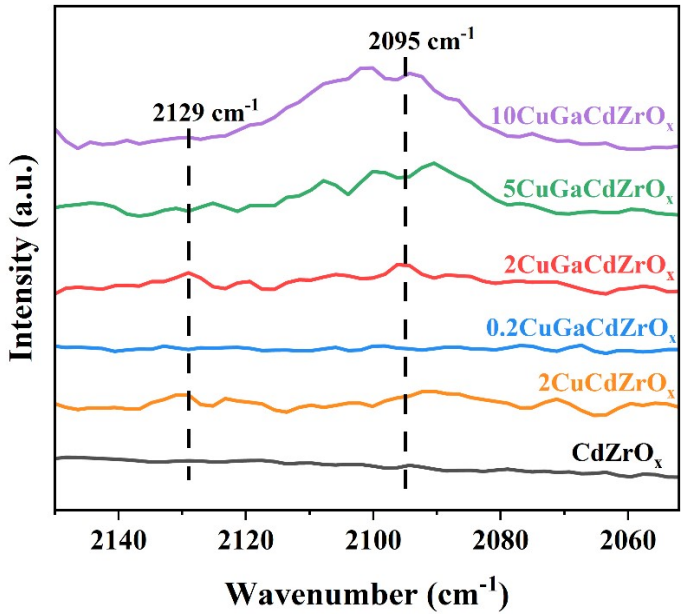

Fig. S8. DRIFTS spectra of CO adsorption on the reduced $CdZrO_x$ and *n*$CuGaCdZrO_x$ catalysts.

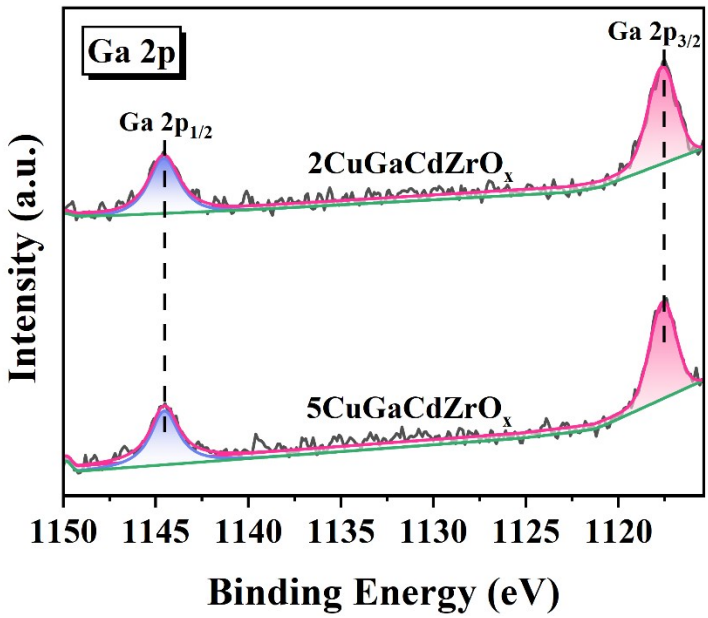

Fig. S9. XPS spectra of Ga 2p of $2CuGaCdZrO_x$ and $5CuGaCdZrO_x$ catalysts.

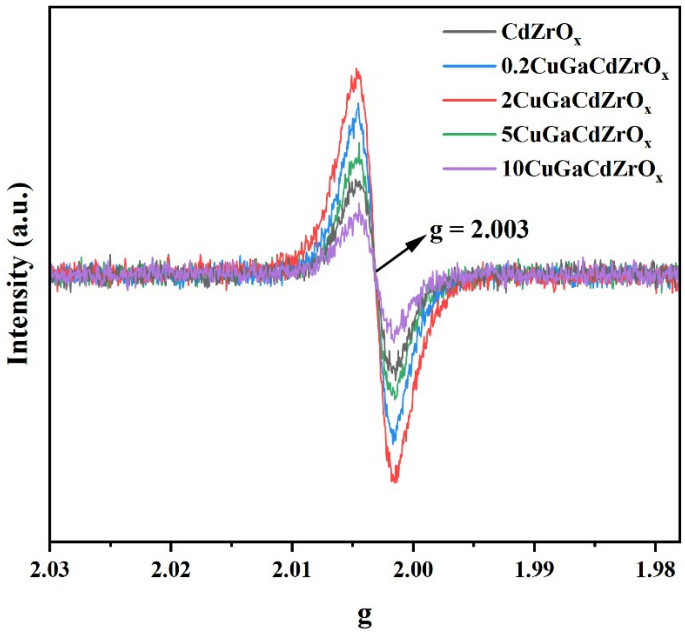

Fig. S10. EPR spectra of the reduced $CdZrO_x$ and *n*$CuGaCdZrO_x$ catalysts.

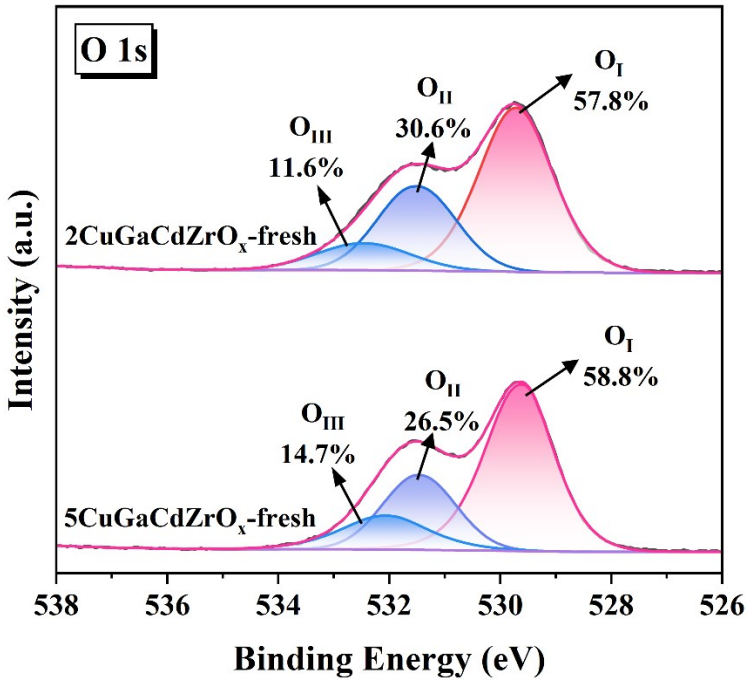

Fig. S11. XPS spectra of O 1s of fresh $2CuGaCdZrO_x$ and $5CuGaCdZrO_x$.

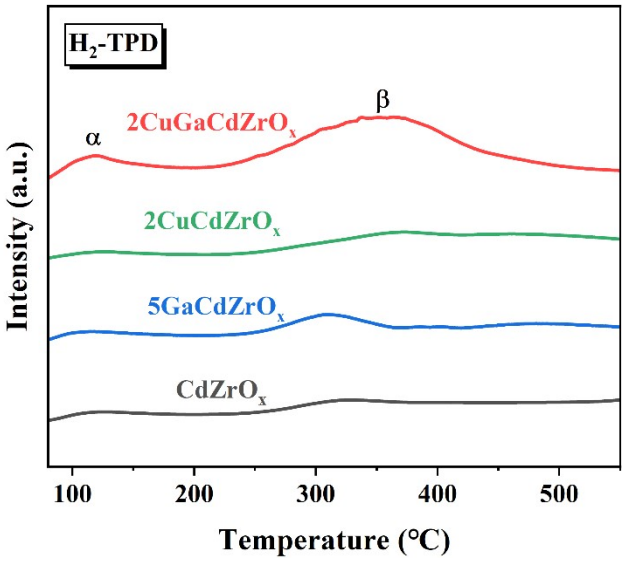

Fig. S12. H_2-TPD profiles of various catalysts.

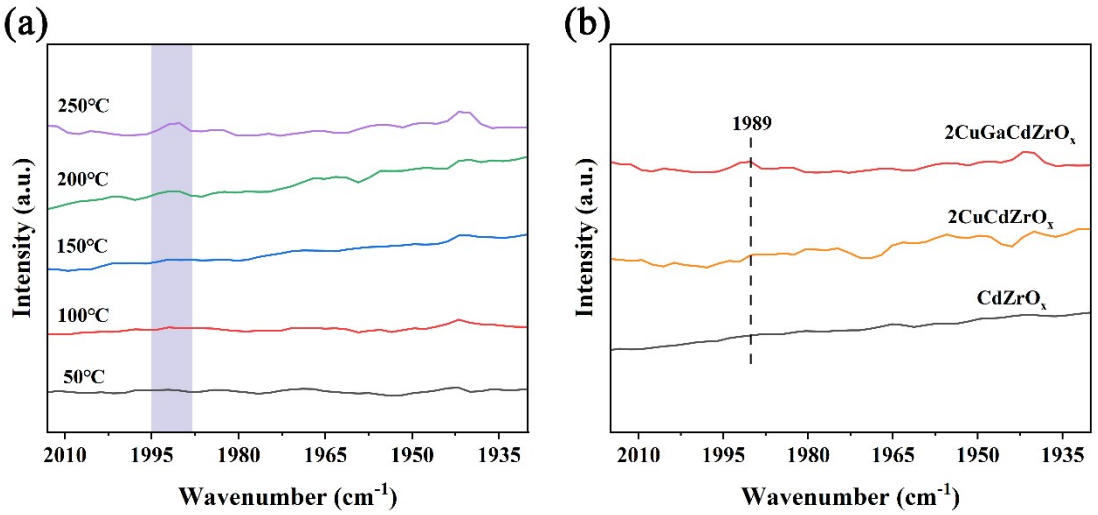

Fig. S13. (a) In situ FTIR spectra for H_2 activation on the $2CuGaCdZrO_x$ catalyst at 50-250 °C. (b) In situ FTIR spectra for H_2 activation on the $CdZrO_x$, $2CuCdZrO_x$ and $2CuGaCdZrO_x$ catalyst at 250 °C.

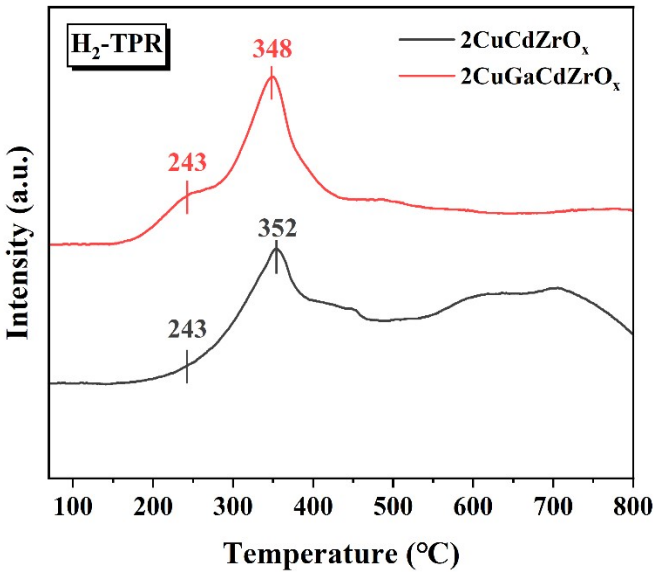

Fig. S14. H_2-TPR profiles of $2CuGaCdZrO_x$ and $2CuCdZrO_x$ catalysts.

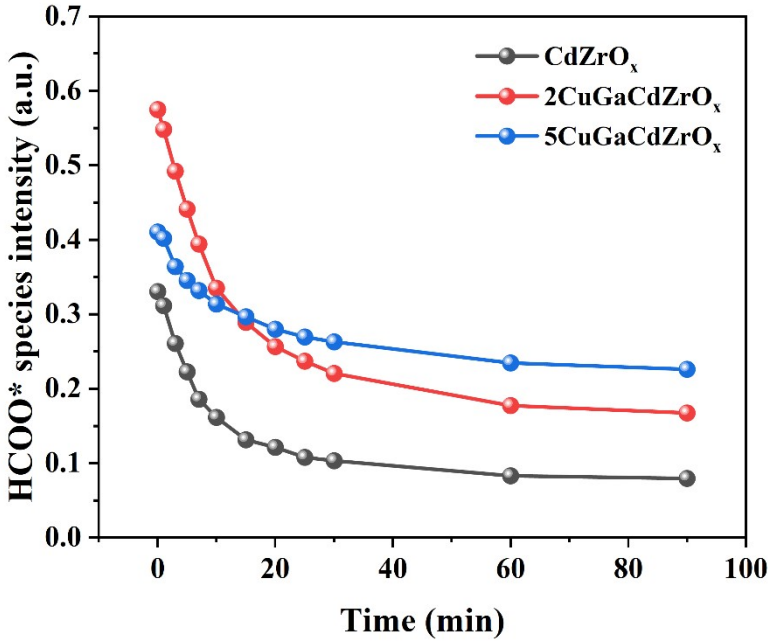

Fig. S15. Variation of IR peak intensities of HCOO* (1589 cm^{-1}) over $CdZrO_x$ $2CuGaCdZrO_x$ and $5CuGaCdZrO_x$ under H_2 sweep after the reaction. Reaction conditions: 280 °C, 0.1 MPa.

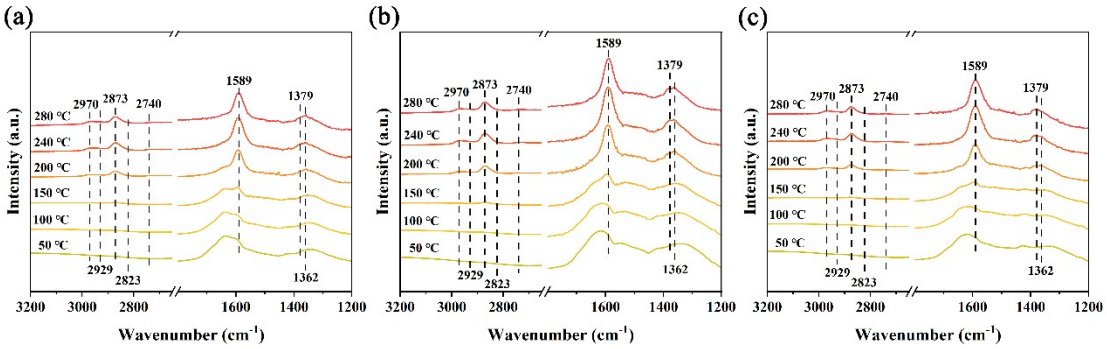

Fig. S16. In situ DRIFTS spectra of the CO_2 + H_2 reaction over the (a) $CdZrO_x$, (b) $2CuGaCdZrO_x$ and (c) $5CuGaCdZrO_x$ solid solution catalysts at various temperatures. Reaction conditions: 50-280 °C, 0.1 MPa, H_2/CO_2 = 3:1.

References

[1] X. Zhang, Q. Kang, W. Wang, K. Lin, D. Feng and B.J. Ma, *J. Environ. Chem. Eng.*, 2025, **13**, 116393.

[2] X. Mao, Y. Zhang, Y. Xu, Y. Zhou, K. Zhuang, K. Shen and S.P. Ding, *Catal. Sci. Technol.*, 2024, **14**, 419-430.

[3] X. Ma, X. Li, X. Yang, X. Tian, H. Zhan, W. Wang, P. Lv and B.J. Ma, *Fuel.* 2023, **346**, 128376.

[4] X.Y. Han, T.T. Xiao, M.S. Li, Z.W. Hao, J.Y. Chen, Y.T. Pan, X.H. Zi, H. Zhang, S.B. Xi, H.M. Wang, S. Kawi and X.B.Ma, *ACS Catal.*, 2023, **13**, 13679-13690.

[5] W. Li, K. Wang, J. Huang, X. Liu, D. Fu, J.L. Huang, Q.B. Li and G.W. Zhan, *ACS Appl. Mater. Interfaces.* 2019, **11**, 33263-33272.

[6] J.J. Wang, C. Tang, G.N. Li, Z. Han, Z.L. Li, H.L. Liu, F. Cheng and C. Li, *ACS Catal.*, 2019, **9**, 10253-10259.

[7] C. Temvuttirojn, Y. Poo-Arporn, N. Chanlek, C.K. Cheng, J. Limtrakul and T. Witoon, *Ind. Eng. Chem. Res.*, 2020, **59**, 5525-5535.

[8] M.S. Frei, C. Mondelli, A. Cesarini, F. Krumeich, R. Hauert, J.A. Stewart, D.C. Ferre and J.P. Ramirez, *ACS Catal.*, 2020, **10**, 1133-1145.

[9] D. Xu, X.L. Hong and G.L. Liu, *J. Catal.*, 2021, **393**, 207-214.

[10] J.P. Zhang, X.H. Sun, C.Y. Wu, W.Q. Hang, X. Hu, D.W. Qiao and B.H. Yan, *J. Energy Chem.*, 2023, **77**, 45-53.

[11] J.L. Song, B. Chen, J.J. Bian, Y.M. Cai, S. Ali, D.R. Cai, B.Y. Zheng, J.L. Huang

and G.W. Zhan, *ACS Appl. Nano Mater.*, 2024, **7**, 19677-19687.

[12] Z.H. Huang, X.Y. Wang, W. Na, X.Y. Ling, X.P. Sun, R.Q. Chen, W.G. Gao and H. Wang, *Appl. Catal., A-Gen.*, 2026, **709**, 120668.

[13] J.Y. Zuo, W. Na, P.Y. Zhang, X.L. Yang, J.L. Wen, M. Zheng and H. Wang, *Mol. Catal.*, 2022, **526**, 112357.

[14] X. Li, Z.X. Feng, H.J. Lu, X.L. Hong, G.C. Li and S.C.E. Tsang, *J. Mater. Chem. A*, 2025, **13**, 20542-20551.

[15] J. He, H.X. Wang, Y. Wang, Y.R. Zhang, Y. Li, L.B. Zhang, Y.Y. Wang, C,L. Yu, S.H. Jia, Q.L. Qian and B.X. Han, Appl. Surf. Sci., 2024, **664**, 160198.

[16] Z.Q. Yan, Y.H. Tian, X.H. Guo, Y.Y. Song, X.Y. Wang, P.W. Li, R.W. Yao, H.Y. Ban and C.M. Li, *Chem. Eng. J.*, 2026, **529**, 172971.

[17] X.Y. Han, M.S. Li, Z.W. Hao, J.Y. Chen, S.X. Tang, Z.M. Zhang, T.T. Xiao, W.Y. Jia, M.C. Chen, P.J. Gao, Y.R. Bai, S.Y. Wang, S.B. Xi, K.H. Lim, Y. Wang, S. Kawi and X.B. Ma, *ACS Catal.*, 2025, **15**, 15141-15152.

[18] D.L. Mao, H. Zhang, J.X. Zhang and D.F. Wu, *Chem. Eng. J.*, 2023, **471**, 144605.

[19] P.C. Luo, P.X. Shi, Z.Q. Yan, J.H. Han, J.J. Wang, Y.C. Li, H.Y. Ban, W.J. Cai and C.M. Li, *Appl. Catal., A-Gen.*, 2025, **689**, 120006.

[20] S.H. Xiong, Y. Lian, H. Xie and B. Liu, *Fuel*, 2019, **256**, 115975.